Nanocrystal symmetry breaking and accelerated solid-state diffusion in the lead-cadmium sulfide cation exchange system

Andrew Nelson,[a] Shreyas Honrao,[a,b] Richard G. Hennig,[a,b] and Richard D. Robinson[a,‡]

[a] Department of Materials Science and Engineering, Cornell University, Ithaca, NY 14853, USA.

[b] Department of Materials Science and Engineering, University of Florida, Gainesville, FL 2611, USA

‡ Corresponding author. Email: rdr82@cornell.edu

Abstract

The phenomenology of solid-state transformations in nanoparticles is important for applications utilizing their reactivity and for investigations into how nearby interfaces interact with the defects responsible for mass transport. We directly interrogate the structure and reaction kinetics of lead sulfide (PbS) nanocrystals undergoing cation exchange in organic solution to cadmium sulfide (CdS) *via* x-ray diffraction (XRD). The epitaxial relationship of zincblende CdS to rocksalt PbS breaks the overall symmetry of the core-shell nanocrystal without requiring the loss of unit cell symmetry, leading to anomalous peak shifts in the diffraction pattern. Conversion occurs in three stages: (1) surface exchange to form a metastable rocksalt CdS shell, (2) crystallization of this shell to zincblende, and (3) diffusive transport of ions through the completed shell. The interdiffusion coefficient, $\tilde{D}$, for ions diffusing through the shell follows the Arrhenius relationship with an activation energy of 160-180 kJ mol^{-1}, which exceeds that observed in many other experiments in diffusion in nanoparticles and is similar to values measured in bulk solids, suggesting the barrier to exchange is dominated by the energies of point defect formation rather than surface-bound reactions. However, the magnitude of $\tilde{D}$ is larger by four orders of magnitude or more compared to the slowest diffusing species in our system (self-diffusion of Cd in CdS). This surprising result suggests interdiffusion is enhanced in nanocrystals, and possible mechanisms include high concentrations of induced extrinsic defects and increase in the diffusive jump length through high-diffusivity paths. Cation exchange illustrates that the distinction between chemical diffusion in a potential gradient and diffusion at thermodynamic equilibrium has not been fully appreciated. Acceleration of interdiffusion in core-shell nanoparticles due to large chemical potential gradients will be important for understanding for nanoscale heterostructure formation and stability.

1. Introduction

The kinetics of solid-state reactions and ionic transport *via* diffusion at the nanoscale are difficult to quantify, owing to the paucity of suitable high-resolution techniques for precisely measuring factors such as phase fraction, interface depth, and composition gradients in nanostructures, especially *in situ*. Such measurements are of great relevance for controlling and predicting the form, function, and stability of nanomaterials. Of concern is whether experiments to determine the dominant defects and their mobilities made in bulk solids may be extrapolated down to length scales (<1-10 nm) relevant for nanostructure growth and modification.[1] A direct demonstration of the solid-state reactivity of nanocrystals (NCs) is seen in the well-researched process of cation exchange, whereby the introduction of a new cation from the solution or vapor phase displaces the existing cations in a compound semiconductor nanocrystal.[2, 3] Much

research has been conducted on an empirical basis using phase transformations by way of ion diffusion to produce novel nanostructures[2-6] with desirable features such as enhanced luminescence,[7] metastable phases,[5] controlled dopant concentrations,[8] and well-ordered epitaxial interfaces.[4, 9]

The diffusion processes that contribute to the formation of these new structures in cation exchange have so far not been systematized. Unresolved factors include: which phase in a heterostructure serves as the primary transport layer for incoming ions, what form of defect the ions take, and from which surfaces the defects originate. Some predictions have been made as to how atomic transport behavior in nanocrystals might change.[10] For example, free surfaces have been predicted to substantially affect the energetics of defect formation and motion in nanocrystals.[11, 12] High-quality kinetic data are necessary to verify these conjectures.

Probes of phase transformation kinetics in cation exchange begin with a nanocrystal precursor having a simple structure and a well-established synthetic chemistry in addition to a cation exchange reaction with kinetics slow enough to allow direct interrogation of the structure by powerful, established methods such as x-ray diffraction (XRD). Both of these requirements are met by the exchange of colloidal lead sulfide (PbS) NCs to cadmium sulfide (CdS) *via* treatment of the NCs with Cd^{2+} salts in organic solution at moderate to high temperatures (100-200°C). This reaction and its variants have been investigated by numerous groups as a route to improving the luminescence and stability of promising lead chalcogenide materials.[13-16] Outstanding questions include the possible existence of metastable phases during cation exchange,[17] the contributions of different crystal surfaces,[18, 19] and the reason for rapid increase in sample polydispersity that accompanies the reaction.[20]

In this work, we use *in situ* XRD to measure the kinetics of phase transformation in the cation exchange reaction PbS (NC) + $Cd(oleate)_2$ → PbS@CdS (core-shell NC) + $Pb(oleate)_2$. We find that the exchange reaction is resolvable into three distinct thermally activated transformation stages, which are described in **Fig. 1**. We attribute these stages to the following processes: A) an initial adsorption of ions onto the NC surface to form a conformal CdS phase in the rocksalt structure (hereafter rs-CdS), B) the recrystallization of this phase into the zincblende structure (hereafter zb-CdS), and C) diffusion-controlled growth of the zb-CdS shell. From the kinetics of the diffusion-controlled stage, we can calculate a value for the activation energy of chemical (inter)diffusion for the rate-limiting species in the zb-CdS shell of around 160-180 kJ mol^{-1} (1.7-1.8 eV $atom^{-1}$). This value substantially exceeds previously reported activation energies for cation exchange in nanoparticles[1, 21, 22] and approaches reported activation energies for point defect migration in the bulk from high-temperature experiments.[23] However, the interdiffusion coefficients measured here still exceed those of self-diffusion coefficients of Cd in CdS from high-temperature data by four or more orders of magnitude.

We also find line shifts in the diffraction patterns of epitaxial PbS@CdS core-shell NCs that indicate the breaking of the cubic symmetry of the NC structure. This appearance is deceptive, however, and we explain using kinematical diffraction theory that the commensurate, offset relationship between the Pb (rocksalt) and Cd (zincblende) sublattices gives rise to a phase factor in the diffracted intensity that results in an apparent peak shift depending on the particular reciprocal lattice vector.[24] The interpretation in reciprocal space of complex NC structures that appear to have undergone, for example, tetragonal[25] or rhombohedral[26] distortions must therefore be done with the knowledge going forward that peak shifts do not necessarily indicate a change in the unit cell symmetry for the constituent phases.

2. Results and Discussion

2.1. Phase relations by XRD intensity quantification

We characterize the structure of PbS@CdS core-shell NCs *via in situ* XRD during cation exchange over a range of temperatures (100-200°C, in increments of 20 or 50°). Monodisperse PbS NCs 7.1±0.4 nm in diameter (**Fig. S1**) were prepared by a previously described procedure[27] and treated with a slight excess of Cd^{2+} ions in the form of Cd oleate (molar ratio, Pb:Cd, of about 1:1.2) in hydrocarbon solution. Experimental details are given in the **Supporting Information** (**Table S1**). XRD shows that pure PbS NCs transform into PbS@CdS core-shell NCs with zb-CdS as their majority component as the reaction proceeds. We did not observe any wurtzite CdS peaks. The data are characterized by complex and non-monotonic changes in the positions, relative intensities, and widths of the three strongest reflections from the initial PbS rock salt phase, namely the (111), (200), and (220) peaks. An example of the XRD patterns from a typical measurement (at 200°C) is shown in **Fig. 2** at left. Patterns are plotted as a function of the momentum transfer, Q, which incorporates the Bragg scattering angle, θ_B, and the x-ray wavelength, λ:

$$Q = \frac{4\pi \sin \theta_B}{\lambda} \qquad (1)$$

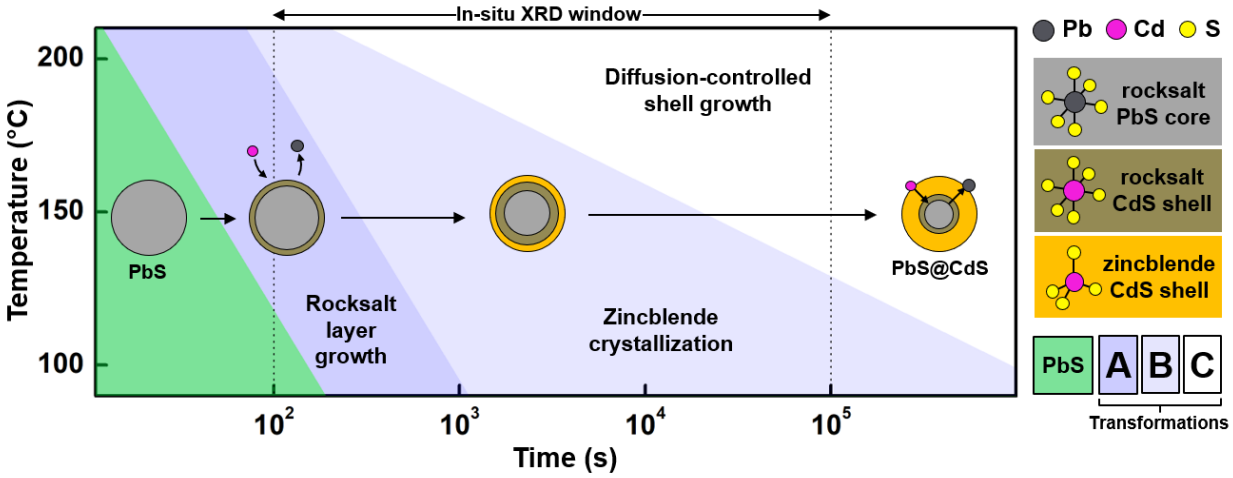

Figure 1. Schematic of isothermal transformation regimes observed with in-situ XRD during the cation exchange of PbS nanocrystals (NCs) with Cd^{2+} at 100-200°C. First, Cd^{2+} rapidly adsorbs to the NCs at all temperatures. A thin shell of rocksalt CdS then develops, which gradually crystallizes to zincblende CdS. At high temperatures, the growth of thicker zincblende shells is kinetically accessible. The stages of the reaction (A, B, C) are detailed in the text.

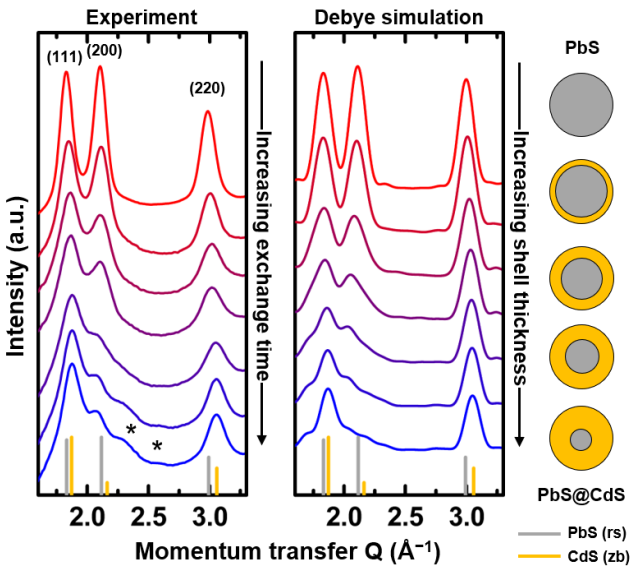

Figure 2. X-ray data (left) from the cation exchange of Cd^{2+} with PbS NCs at 200°C. The intensity of the (200) peak decreases relative to that of (111) during shell growth, consistent with a transformation from rocksalt PbS (gray vertical lines, JCPDS 01-072-4873) to zincblende CdS. The reflection corresponding to the (200) plane shifts to smaller angles and splits, while the (111) and (220) reflections shift to larger angles in accordance with the smaller lattice constant of CdS (yellow vertical lines, JCPDS 01-075-0581). Debye scattering simulations (right) of PbS@CdS core-shell NCs with varying zincblende CdS shell thicknesses show that the anomalous peak shifts and splittings arise from diffraction effects dictated by the commensurate relationship between the two phases. Asterisks mark a possible CdO degradation product. Diagram colors (far right) as in **Fig. 1**.

The relative intensities of the strongest diffraction peaks can be used as a proxy for the total extent of the phase conversion.[28, 29] Here, the amplitudes of (111) and (200), I_{111} and I_{200}, respectively, can be used to track the contributions from the PbS and CdS. In as-synthesized PbS NCs, I_{111} and I_{200} are nearly equal, with I_{111}/I_{200} being about 0.96-0.98, within the margin of error of the bulk value of 0.96 (JCPDS 01-072-4873) (**Fig. 3** and **S2**). Changes in I_{111}/I_{200} following addition of Cd^{2+} are strongly temperature dependent. At low temperatures I_{111}/I_{200} initially decreases to approximately 0.92-0.93, and afterwards the ratio slowly and monotonically increases, remaining below 1.1 at 120° and 1.5 at 150°C, even after 12 or more hours of exchange. At high temperatures (180-200°C), however, cation exchange is much faster, and the initial decrease in I_{111}/I_{200} is not seen. The minimum observed in I_{111}/I_{200} for reactions at low temperature occurs at the first data point, less than 60 s after the start of the reaction, so that if a minimum in I_{111}/I_{200} occurs at higher temperatures, the temporal resolution of the experiment is too low to observe it. **Fig. S2** shows that at the lowest temperatures (100°C), I_{111}/I_{200} remains at a low value (0.9) without beginning to increase again, indicating the thermal energy is insufficient to effect further growth of the shell. At high temperatures I_{111}/I_{200} increases rapidly and monotonically, reaching a limiting value of 3.5-4 after ~4 h at 180°C and less than 1 h at 200°C. The nominal end-product of the cation exchange reaction, zb-CdS, has an I_{111}/I_{200} of about 4.6 (JCPDS 01-075-0581, horizontal line at top of **Fig. 3**). Our experimentally-found smaller value (3.5-4) may be due to a decrease in the reaction driving force as the free Cd concentration becomes small. A continuous transformation from PbS to zb-CdS would result in I_{111}/I_{200} increasing, slightly nonlinearly but monotonically (*i.e.*, without an initial decrease).[28, 29] Thus, at low temperatures, our observed trends for I_{111}/I_{200} are not in accordance with a simple linear combination of PbS and zb-CdS. However, these trends become explicable after considering previously hypothesized metastable phases during cation exchange. The high-pressure rocksalt phase of CdS (rs-CdS), with a lower I_{111}/I_{200} of about 0.6 (JCPDS 01-071-4151, horizontal line at bottom of **Fig. 3**), has been proposed as an intermediate phase.[17, 30] Our

experimental results suggest that, at low temperatures and/or small degrees of cation exchange, Cd is indeed introduced to the NCs as rs-CdS and causes an initial decrease in I_{111}/I_{200}. Because I_{111}/I_{200} increases at longer times, however, the final CdS phase formed must be zincblende.

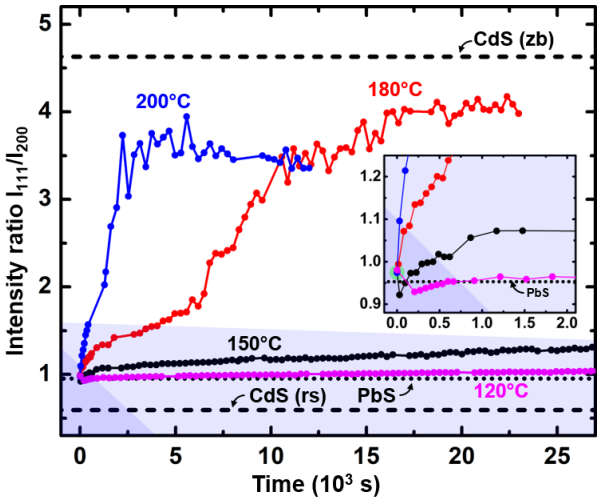

Figure 3. Intensity ratio I_{111}/I_{200} of the first two diffraction peaks (111) and (200) during cation exchange of PbS to CdS. The bulk values for PbS (0.96, rocksalt phase) and CdS (4.6, zincblende phase (zb), top, and 0.6, rocksalt phase (rs) bottom) are indicated by the dashed lines. At low temperatures and short exchange times, a drop in the intensity ratio occurs (inset), consistent with a PbS-to-rocksalt-CdS transformation, but the direction of I_{111}/I_{200} soon reverses, indicating the remainder of the CdS forms in the zincblende phase. The stages of the reaction (as in **Fig. 1**) are indicated.

2.2. XRD peak shifts and symmetry breaking

The changes in relative intensities are initially accompanied by shifts of all three reflections to significantly larger scattering angles Q (**Fig. 4**, **S3**), showing a decrease in the average lattice parameter, a_0, of the NCs in accordance with the smaller (by a factor, Δd/d, of -2.2%) lattice constant of zb-CdS (5.81 Å) compared to that of PbS (5.94 Å). This immediate shift of ΔQ = 0.015 to 0.02 $Å^{-1}$, or Δd/d = -0.3 to -0.5%, occurs in the first several minutes of the reaction at all temperatures. Thereafter, the (111) and (220) peaks move more gradually to larger angles, remaining intermediate in position between the bulk values for the two endmembers (PbS and zb-CdS). Surprisingly, after an initial increase in diffraction angle, the (200) instead begins to move to smaller angles. This shift to smaller angles is very gradual (<0.005 $Å^{-1}$, Δd/d = -0.1 to -0.2%, over 12 h) at low temperature, but at higher temperatures (180-200°C) the (200) can shift by up to 0.02 $Å^{-1}$ (Δd/d > +1%) relative to the starting PbS. For phases of cubic symmetry, such as the nanocrystal component PbS/zb-CdS phases, the *d*-spacings assume a relationship to the lattice constant a_0 for the plane with Miller indices (hkl): $d_{hkl} = a_0 / \sqrt{h^2 + k^2 + l^2}$. Since it is presumed that the deposition of CdS on PbS (and thus the development of any resulting strains) is nearly isotropic during cation exchange, it follows that Δd/d should be the same for all peaks and that changes in the lattice parameter in a cubic structure should shift all peaks in the same direction in reciprocal space. This conflicts with our experimental results, so we necessarily conclude that cubic symmetry is lost in the core-shell NCs later in cation exchange. Reports of symmetry breaking in NCs in recent years have straightforwardly attributed this mismatch between peak positions to a distortion of the unit cell[25, 26, 31] (*e.g.* tetragonal or rhombohedral). We will investigate this possibility shortly.

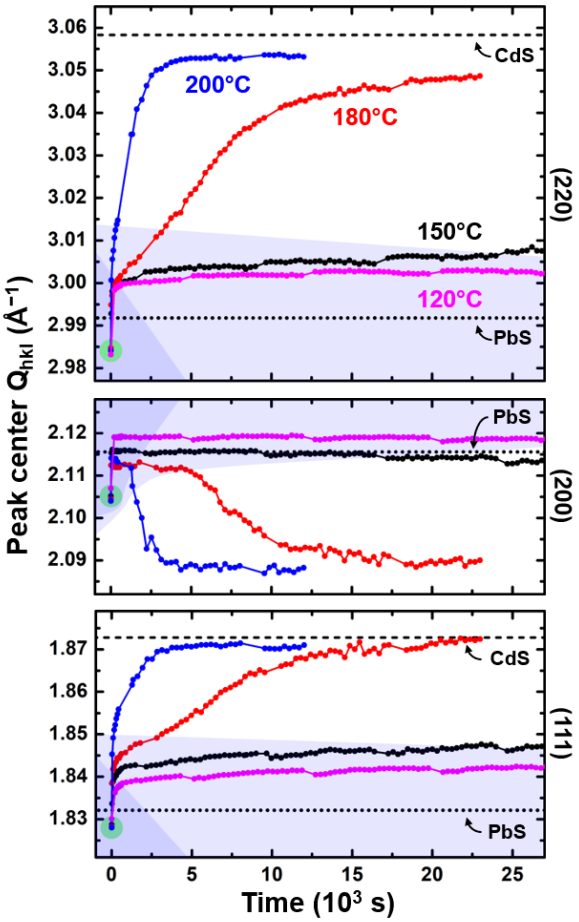

Figure 4. Fitted (111), (200), and (220) peak positions from in-situ XRD data for the cation exchange of 7 nm PbS NCs to CdS. A continuous shift to larger angles for (111) and (220) indicates a change to interplanar spacings more like those of CdS. The (200) peak briefly follows the same behavior as (111) and (220), but then reverses direction. The broken horizontal lines indicate the estimated line positions for bulk PbS (rocksalt) and CdS (zincblende). Stages in the reaction (as in **Fig. 1**) are indicated.

Along with the anomalous shift of (200), at long exchange times (hours) for temperatures of 150-200°C we observe the appearance of an additional reflection (Q ~ 2.26 to 2.38 Å^{-1}) at angles larger than the (200) peak (Q ~ 2.08 to 2.12 Å^{-1}). This reflection's position is not consistent with a peak from either a wurtzite CdS (JCPDS 01-070-2553) phase or from an isolated, unstrained zb-CdS (200) peak. It is consistent with the (111) reflection at 2.32 Å^{-1} from a small amount of rocksalt CdO (lattice parameter 4.70 Å, JCPDS 00-005-0640), but the corresponding CdO (200) reflection, which should occur at 2.67 Å^{-1}, appears to be very weak or absent in spite of its comparable theoretical intensity to CdO(111) (I_{111}/I_{200} = 1.14 for CdO). The appearance of CdO might be caused by thermal degradation of the Cd oleate at higher temperatures[32] or by oxidation due to the imperfect sealing of the reactor. To fit these patterns with the additional peak (for temperatures 150-200°C) we added an additional peak for the contaminant, which greatly improved the quality of the fits for the peak shapes while preserving the trends of the peak shifts and intensities (**Fig. S4**). We confirm below that formation of rs-CdS from cation exchange should result in a monotonic increase of reflection angle for (111), (200), and (220) and that, in the case of zb-CdS, (200) is expected to move to smaller angles. Our experimental data for the peak positions follow the same trends as observed for the relative intensities, indicating the formation of a rocksalt-like CdS phase followed by the gradual growth of the more thermodynamically stable zincblende phase.

2.3. Theoretical predictions: Debye scattering simulations

To quantitate the overall evolution of peak intensities and shifts for the core-shell NCs, we simulate the system by building an atomic model consisting of spherical particles of PbS and hollow spherical shells of zb-CdS having a completely commensurate anionic sublattice. Each phase is assigned its bulk lattice parameter and is not relaxed for lattice matching at the interface. For 7 nm core-shell particles, the models comprise about 7000 atoms. We then calculate the diffraction patterns at varying degrees of cation exchange by means of the Debye scattering equation from a series of core-shell particles with progressively thicker zb-CdS shells (**Fig. 2**, right, **Fig. 5**, and **Fig. S5**). Results from these simulations show that I_{111}/I_{200} should increase monotonically with shell thickness (**Fig. S5**), in agreement with the experimental data at longer times. The experimental limiting value of I_{111}/I_{200} at high temperature is about 3.5, corresponding to a conversion fraction of about 90%. We cross-checked this value of the conversion fraction against the value determined from the calculated dependence of (220) peak position on conversion (**Fig. 5e**) and found them to be reasonably consistent. Importantly, the patterns also replicate the anomalous movement of the (200) peak to smaller angles (**Fig. 5d**, filled circles). However, for simulated zb-CdS shells at low conversion fractions, peak parameter trends disagree somewhat with experiment. Simulated peaks do not move uniformly to larger scattering angles: (111) does not change position and (200) only moves to smaller angles, while (220) moves to larger angles, its position being nearly linearly proportional to the phase fraction. Finally, the theoretical I_{111}/I_{200} does not decrease (**Fig. S5a**). Thus, the simulated diffraction patterns indicate that the zb-CdS phase may not account for the trends in the peak parameters early in the experiments but is consistent with the results at larger conversion fractions.

To confirm alternative hypotheses[17, 30] about the phase of the CdS and investigate the deviation in experimentally determined parameters at short exchange times from those from the Debye simulations, we also calculated the patterns with a rs-CdS shell. We adopted for this structure the same lattice parameter used for zb-CdS. Results from our model find that all peaks should shift smoothly to larger angles (**Fig. 5c-e**, open circles) and that I_{111}/I_{200} should decrease (**Fig. S5b**). That is, for a rs-CdS shell, the trends in intensities and peak positions are the opposite of those for the zb-CdS case. We found that our experimental data are consistent with a metastable rs-CdS shell during the initial growth of the CdS layer. The experimental magnitude of the initial isotropic shift of the NC lattice parameters to larger angles, compared to that from the simulations, suggests a total conversion fraction of ~10-20% total conversion of the NCs at maximum. This conversion fraction is in reasonable agreement with that derived by comparing our measured change in I_{111}/I_{200} from 0.97 to 0.92 to that from the simulations for a rocksalt CdS shell. A conversion fraction of 20% of the NC represents a shell thickness of about 0.25 nm, less than one unit cell, for NCs 3.5 nm in radius. It is possible that this thin rocksalt layer persists as an interlayer between PbS and zincblende CdS as the cation exchange progresses, but the uncertainty in the data makes an interlayer's presence difficult to confirm.

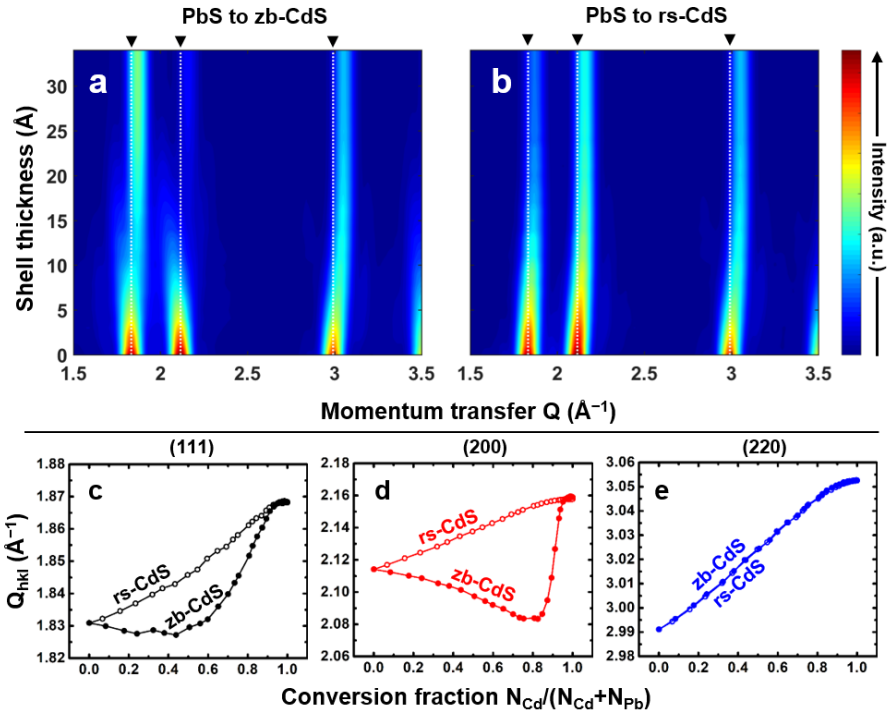

Figure 5. (a,b) Debye scattering equation simulations of the diffraction patterns for PbS@CdS core-shell NCs with increasing thickness of CdS shell. With a zincblende CdS shell (a) the peak centers of the (111) and (200) reflections have a complex and non-monotonic relationship to the total conversion fraction (c-d, filled circles) and are split/broadened. However, when the CdS shell has the rocksalt phase (b), all peaks move smoothly and monotonically to larger angles (c-d, open circles). Black arrows and dashed lines indicate the reference positions for rocksalt PbS. Regardless of the phase chosen for CdS, (220) follows the same nearly linear relationship between position and phase fraction (e) and remains unsplit (a-b).

2.4. Nanocrystal disorder and peak width

Details of nanocrystal structure are also reflected in changes in the width of diffraction peaks (**Fig. 6** and **S6**). In as-synthesized PbS, peak broadening is somewhat greater than expected for a 7 nm nanocrystal (effective domain size is ~5 nm). This intrinsic broadening does not change with time or temperature and may arise from an instrumental contribution (**Fig. S7**). Additional broadening occurs immediately following the introduction of CdS (**Fig. 6** and **S6**), which is not predicted by the Debye simulations for PbS@rs-CdS rocksalt NCs for small degrees of exchange (**Fig. S8**). We therefore suggest that the formation of the initial shell adds high levels of inhomogenous strain, especially at the surface. Such strains might be introduced by non-uniform decoration of the surface with CdS domains large enough (>1 monolayer) to require defects to accommodate them. To explain the presence of large enough domains, we note that previous work found that the presence of excess ligand (Pb oleate) remodeled the surface of PbSe NCs, even at room temperature, by altering the relative proportions of each facet.[33] This effect requires the redistribution of a significant fraction of the cations around the NC if anion number is to be conserved. As a result, it is possible that incoming Cd could take the place of Pb during faceting, which could redistribute the particle mass rapidly enough to

form the required CdS domains. Alloying of PbS and CdS[30] may also be possible through this mechanism, thereby introducing strain *via* a $Pb_{1-x}Cd_xS$ shell with a lattice constant smaller than that of PbS. For the high degree of exchange (10-20%) in the first step of the reaction to occur, Cd must have considerable solubility in PbS NC surfaces, in contrast to the nearly negligible measured low-temperature solubility in bulk (Pb,Cd)S.[34] Increased miscibility of bulk-insoluble components has been previously observed in nanomaterials.[35-37] However, for PbS@CdS observed here, the small experimentally determined decrease in I_{111}/I_{200} at very short exchange times at low temperature is more consistent with a very thin (<0.25 nm) surface alloy layer, so an increase in "bulk" miscibility is not clearly demonstrated.

Not only do the Debye scattering simulations for PbS@zb-CdS (**Fig. 5**) replicate the shift of the (200) reflection to smaller angles in opposition to the movement of (111) and (220), they also show new weak peaks appearing at the tails of (111) and (200), causing them to appear substantially broader (**Fig. S8**). These features do not appear in simulated patterns for rs-CdS shells. We find in the experiment that the widths of (111) and (200) are indeed greater than the width for (220) throughout cation exchange (**Fig. 6**). A possible exception is seen for the case of 180°C at longer exchange times, but as overlap between (111) and (200) is substantial, errors are expected in estimating individual peak widths and their average width is still substantially greater than that of (220).

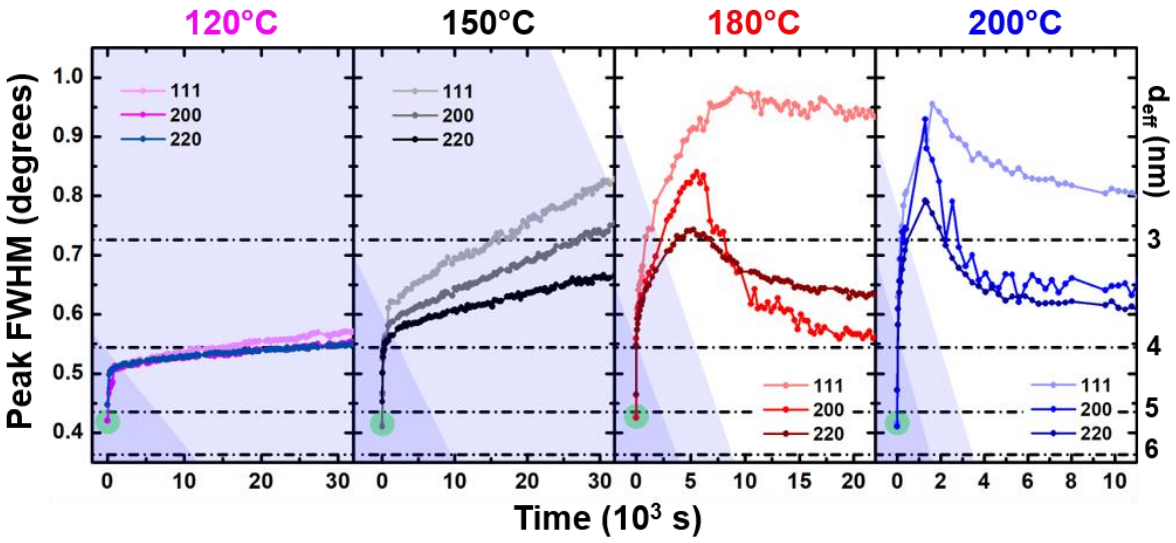

Figure 6. Extracted peak widths for the cation exchange runs from **Fig. 3** for (111) (light-), (200) (medium-), and (220) (dark-colored) reflections. Light horizontal lines give the peak widths estimated from the Scherrer equation ($K = 1$, $\cos\theta_B \approx 1$) for crystalline domains of various diameters d_{eff} (at right). Due to broadening from the thickness of the sample and mismatch between PbS and CdS, the peak widths are larger than expected for particles of 7 nm diameter. Stages in the reaction (as in **Fig. 1**) are indicated.

2.5. DFT calculations of phase stability

To investigate the stability of the rs-CdS layer, we performed density functional theory (DFT) calculations to determine the relative formation energies of PbS–zb-CdS, PbS–rs-CdS,

and PbS–rs-CdS–zb-CdS interfaces. Details on these calculations are provided in the **Supporting Information** (**Tables S2-4**). PbS(100) slabs were layered with 0 to 4 monolayers of rs-CdS followed by 0 to 2 monolayers of zb-CdS (**Fig. S9a**). The relaxed surface energies for these interfaces showed that for the first monolayer of CdS on PbS the rocksalt phase was indeed favored, having an interface energy of 69 meV $Å^{-2}$ versus 86 meV $Å^{-2}$ for the zincblende phase. This trend continued for bilayers of CdS (89 vs. 134 meV $Å^{-2}$ for rocksalt vs. zincblende, respectively). Although the energy difference was less pronounced, a configuration with one rocksalt and two zincblende CdS monolayers had a higher energy than one with two of rocksalt and one of zincblende (161 vs. 154 meV $Å^{-2}$). In terms of energy per monolayer, a surface with only rocksalt layers had the lowest energy at least up to thickness of 1 nm (**Fig. S9b**). Our experimental results constrain the rs-CdS layer to be much thinner, but other work has conjectured that rs-CdS could be destabilized by surface curvature.[17] This would explain the greater stability of thicker rs-CdS epilayers in simulation, where, for reasons of computational expense, we used flat surfaces in one orientation. In general, however, the DFT calculations support the hypothesis that a rs-CdS layer could persist on the PbS surface in the absence of the high pressure normally required to stabilize bulk rs-CdS. Interestingly, in a similar system (PbTe-CdTe) a rocksalt CdTe interface has not been observed despite a much lower mismatch between PbTe and zincblende CdTe.[38] The stabilization of rs-CdS in the PbS-CdS system, despite (or owing to) pronounced lattice mismatch, could provide insight into band engineering[39, 40] for devices using core-shell NCs, since Cd chalcogenides are indirect narrow-gap semiconductors in the rocksalt phase but have a much larger, direct gap in the zincblende phase.[41, 42]

2.6. Origins of apparent symmetry breaking: kinematical diffraction theory

The anomalous shifts and peak broadening indicate that a linear combination of the patterns of the two isolated components cannot model the diffraction pattern due to a non-random relationship between the PbS and CdS lattices. Contributions to the diffracted intensity from core and shell cation pairs (*i.e.*, Pb-Cd pairs) do not reflect either the rocksalt or zincblende symmetries and result in changes in the position and intensities of certain peaks. If there were a random relationship of PbS and CdS domains (no epitaxy), the scattered intensities from PbS and CdS would again be linearly independent, and Bragg reflections would shift monotonically regardless of whether CdS adopted the rocksalt or zincblende phase. These modeling results illustrate dramatically that cross-interactions between separate components of commensurate heterostructures can have significant impact on the structure inferred from a less sophisticated structural analysis.

Fundamentally, the “unusual” diffraction behaviors can be understood to arise from a net translation of one sublattice (Cd) relative to another (Pb). Specifically, in the zincblende phase the cations, adopting tetrahedral coordination, are translated relative to the octahedrally coordinated rocksalt positions in the unit cell along the <111> direction. Previous work in electron microscopy has shown that such displacements between otherwise isostructural diffracting domains, as observed in stacking faults and antiphase boundaries, can lead to splitting of diffraction peaks when the overall size of the diffracting region is small (*i.e.*, most atoms are near the interface).[24] The requirement for splitting of peaks is determined by the criterion $\mathbf{r}_{hkl} \cdot \mathbf{R}$, where $\mathbf{r}_{hkl}$ is the reciprocal lattice vector and $\mathbf{R}$ is the translation vector for a sublattice (**Fig. S10**). If $\mathbf{r}_{hkl} \cdot \mathbf{R}$ is not an integer (that is, the lattice is translated by a non-integer multiple of the plane spacing in that direction), peak splitting results. For adjacent zincblende

and rocksalt cation sublattices sharing a commensurate anion sublattice, $\mathbf{r_{hkl}} \cdot \mathbf{R}$ is ¾ for (111), ½ for (200), and 1 for (220), so that splitting is expected for the first two. We clearly observe splitting of both (111) and (200) in the Debye simulations (**Fig. 2**). However, in the experimental diffraction patterns, the peak splitting is not distinguishable in (111), possibly due to inhomogeneities in the thickness of the CdS layer within (if the core were off-center) or between (if different NCs are converted at different rates) particles, to the presence of significant inhomogeneous strains, or to non-isotropic thermal displacements. The peak at 2.26-2.28 which we previously suggested to be due to CdO may, in fact, result from the splitting of (200), but a definitive assignment remains uncertain.

The contributions to the scattered intensity from commensurate phases in small crystal domains, in which nearly all atoms are close to an interface, are difficult to describe by conventional profile-fitting methods such as Rietveld refinement. These methods assume that the crystal may be described by a single unit cell having translational symmetry in all directions, which is not the case here. As a result, diffraction effects such as peak splitting and anomalous shifts may have been overlooked in previous calculations of nanoparticle scattering patterns. Some studies have attributed anomalous peak shifts in diffraction patterns of cubic materials to a distortion (tetragonal, rhombohedral, *etc.*) of the unit cell,[25, 31] while other workers have noted the influence of core-shell formation and the translation of sublattices.[26, 43] Moreover, the shifts need not be restricted to the cationic sublattice: Bals et al.[44] show that the cation exchange of PbSe to CdSe leads to the formation of a displaced Se lattice in CdSe relative to the parent PbSe sublattice, as well as stacking faults. Our results show that it may not be necessary to change the space group of a single crystal domain to account for these shifts. Instead, an epitaxial domain where one component has a net displacement relative to a perfect extension of the substrate (as in a stacking fault) creates a particle with overall symmetry lower than either of its constituents' space groups without a change in the unit cell symmetry of its constituents. Such displacement disorder effects[45] outside of the bulk crystal diffraction formalism and its corrections (such as the Scherrer equation) have significant implications for studies of epitaxially structured nanoparticles.

2.7. Transmission electron microscopy and Raman spectroscopy

The structure of the nanoparticles may be most directly interrogated using electron microscopy. As-synthesized PbS NCs are single-crystalline and lack extended defects in the core such as stacking faults or twin boundaries (**Fig. 7a**); the high crystallinity leads to sharp and undivided peaks in the Fourier spectrum from images of individual nanoparticles. Following exchange at 150°C for 11 h, the size and shape of the NCs are unaltered, but their degree of crystallinity changes markedly (**Fig. 7b**). This manifests as inhomogeneity of the signal intensity across the particle, indicating variations in the alignment of the zone axis to the beam, and the distortion and bending of lattice fringes. In contrast to previous studies on the PbTe-CdTe exchange system,[20] where lattice mismatch is less than 0.3%, well-resolved core-shell structures with distinct rocksalt and zincblende lattices are not observed so far for thin shells in the PbS-CdS system, which has a much larger mismatch of 2.2%. Anisotropic streaking of the peaks in the Fourier spectrum for the exchanged particles shows that the disorder introduced by the shell is non-uniform, lending credence to our conclusions from the Debye simulations that the CdS layer is epitaxially related to the PbS by a translation vector in the Cd sublattice (**Fig. S10**). The vector necessarily points along one axis of the particle, thereby breaking cubic symmetry,[26] even if a new crystalline phase is not apparent due to the thinness of the shell.

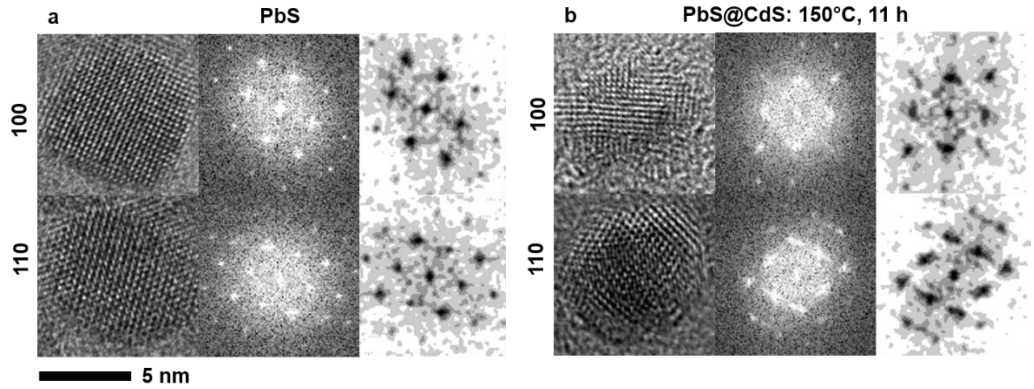

Figure 7. High-resolution TEM imaging of PbS and PbS@CdS nanocrystals. Before transformation, PbS NCs (a) are single-crystalline with no strain gradients, grain boundaries, or stacking faults (left), resulting in sharp peaks in their Fourier transform (center). Following exchange, NCs show structural distortion as evidenced by Moire fringes, (c) reflected in the FT as streaking and splitting of the peaks due to core-shell lattice mismatch. The FTs of (a) and (b) have also been stylized for clarity (right); the zone axes are indicated at left of (a) and (b).

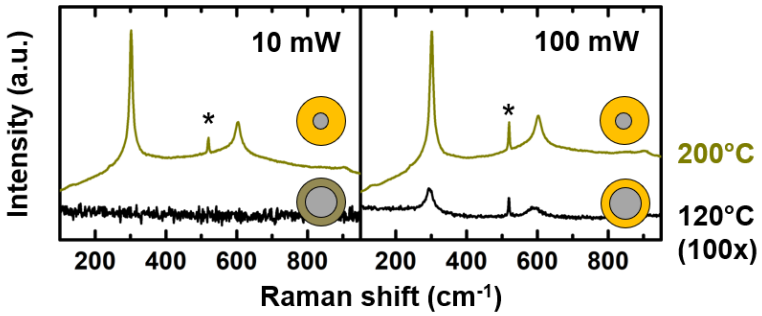

Figure 8. Raman spectra of PbS@CdS nanocrystals, where the CdS shell was grown at the indicated temperature for 1 hour. Zincblende CdS is distinguished by the 1LO line at 300 cm^{-1} and its overtones. NCs prepared at 120°C initially have no Raman signal, but higher laser powers induce crystallization of the rocksalt shell to zincblende. After growth at 200°C, the LO lines are visible even beginning at low laser powers, indicating the crystallization of the shell is thermally activated. The line marked with the asterisk is from the silicon substrate. Argon-ion laser λ_{exc} = 488 nm; diagram colors as in **Fig. 1**.

Raman spectroscopy of PbS and PbS@CdS NCs allows us to definitively identify the CdS phase in thin shells since Raman spectra of materials are highly specific to crystal phase and symmetry. No first-order vibrational modes are expected to be Raman active in bulk PbS (or rs-CdS) owing to symmetry,[46] but signals from PbS nanoparticles arising from surface modes[47] or from photodegradation products[48, 49] have been reported. However, zb-CdS exhibits a clear Raman spectrum with a sharp longitudinal optical (LO) phonon line at about 300 cm^{-1} and its overtones.[50] Shell thickness in Raman characterization experiments was controlled by the reaction temperature during 1 h of cation exchange.

We observed no Raman spectrum from the initial PbS NCs except for weak signals which could be attributed to Pb-O and SO_4^{2-} vibrations at 140 and 960 cm^{-1}, respectively (**Fig. S11**).[48] Raman spectra of PbS@CdS NCs, however, are more complex (**Fig. 8** and **S12**) and depend on growth temperature, time of exchange, and laser power. We first consider samples in which the CdS shell was grown at 120°C. For samples extracted immediately (60s after start of exchange), for which no chemical change has occurred other than the initial adsorption of Cd oleate, we observe no Raman lines from CdS regardless of laser power (**Fig. S12a**). After 300 to 3600 s exchange times, following which the NCs become completely coated with Cd and the slow growth of a CdS shell has begun, no lines are detected at low laser powers (**Fig. S12b-c**). However, after increasing the incident power on the same spot tenfold, the zinc blende LO phonon signature abruptly appears (**Fig. 8**) and persists in the spectrum even if the laser power is reduced again. Evidently, laser heating triggers the irreversible formation of the zb-CdS phase. Laser heating of the core-shell NCs can also be observed from a small shift of 3-5 cm^{-1} in the CdS LO phonon positions to smaller wavenumbers at the highest laser power. Raman spectra thus also point to the existence of a metastable rs-CdS layer crystallizing as zb-CdS at higher temperatures.

The Raman spectra for NCs exchanged at 200°C reflect the much faster cation exchange. After 60 s of growth, the spectra are similar to those for samples exchanged at 120°C for long time periods: the LO phonon is absent at first but appears after laser power is increased (**Fig. S12d**). Samples exchanged for longer times (300-3600 s), however, always show a clear LO phonon peak, even when observation begins at laser powers as small as 0.1 mW (**Fig. S12e-f**). The. On the basis of these observations and the preceding x-ray data, we conclude the initial CdS shell exists in the rocksalt phase, possibly as an alloy phase $Pb_{1-x}Cd_xS$, and that its crystallization to zb-CdS is thermally activated. Shells grown for only 60 s at 200°C precede any of the XRD data points in **Fig. 3**, but laser-induced formation of zb-CdS still occurs. Therefore, this rocksalt phase appears to be an intermediate at all growth temperatures, but the time resolution of in-situ XRD was insufficient to detect it.

Previous work showed that photoluminescence quantum yield for PbS@CdS core-shell NCs was maximized at a particular shell thickness[14] and proposed that this maximum arose from a rs-CdS to zb-CdS phase transformation, which we observe here.[17] A maximum quantum yield at a specific shell thickness has been seen in other core-shell systems[51, 52] and been attributed to the formation of defects due to accumulation of strain energy.[53, 54] Due to the difficulties of incorporating optical observation during the XRD experiment, parallel optical data cannot be given at present, but our XRD results confirm that metastable surface (and possibly interfacial) phases can be observed directly.

2.8. Kinetics: stages of cation exchange

By tracking the XRD peak intensities, positions, and widths for the rocksalt- and zincblende- like (111), (200), and (220) reflections for reactions at several temperatures, we find three stages for the exchange (**Fig. 1**, **3**, **4**, and **6**, with 7.1 nm PbS NCs particles used as the model system), to which we assign the names **A**, **B**, and **C**. At all temperatures there is an initial decrease in unit cell size and increase of peak width which is close to the time resolution of the experiment (much of the change occurs between the zero timepoint and the first data point). This large and isotropic change in lattice parameters, stage **A**, is completed in <300 s and is consistent with an effectively instantaneous introduction of a rs-CdS layer or group of domains

making up about 20% of the NC, which decreases I_{111}/I_{200}. The increase in peak broadening in stage **A** (**Fig. 6**) also suggests the introduction of significant inhomogeneous strain.

In the subsequent stage **B** (t > 300 s), at low temperatures (120° and 150°C) peak positions and widths change much more slowly than in stage **A**, giving the kinetic curves an overall L-shape. I_{111}/I_{200} begins to increase again, while the positions of the peaks are nearly constant ((200) moves very slightly to smaller angles), indicating stage **B** is primarily a recrystallization of the rs-CdS surface to zb-CdS due to the accumulation of strain energy.[53] As all peaks are still seen to shift (**Fig. 5e** would lead us to believe the (220) position is essentially independent of CdS phase), during stage **B** shell growth still continues, although more slowly.

At higher temperatures, stage **C** becomes thermally activated and comes to dominate the exchange, making the contribution of stage **B** difficult to discern. The onset of stage **C** is marked by an inflection in the shape of the curve (*e.g.* 180°C curve in **Fig. 4**). Such inflections were observed during kinetic experiments on ion exchange in NCs by other workers and were also attributed to changes in transport processes.[55] During stage **C** (t > 300 s at high temperatures) the zb-CdS phase grows more rapidly and the conversion is able to run nearly to completion, so that at 200°C the (111) and (220) positions approach those of the pure zb-CdS phase after less than 1 h. The value of I_{111}/I_{200} and the position of (220) at the endpoint of the 200°C reaction are, from the Debye simulations (**Fig. 5**), consistent with a conversion fraction of 90%. The onset of stage **C** also changes the behavior of the peak width, which begins to decrease again (**Fig. 6** and **S6**). The widths of all peaks reach a maximum at about 1400 s at 200°C and at 5000 s at 180°C, which is consistent with overlapping, displaced peaks' having a maximum apparent width when their intensities are comparable. After undercoordinated surface cations are replaced during **A** and **B**, new cations must travel through the shell by way of energetically unfavorable defects, so slow ionic transport becomes the rate-limiting step in cation exchange during stage **C**.[56]

2.9. Quantitation of cation exchange kinetics: stages A and B

We now examine in more detail the changes of peak positions in the experimental diffraction patterns. Debye simulations showed that the (220) peak does not split and that its peak center, Q_{220}, has a nearly linear relationship to the conversion fraction (**Fig. 5e**). Accordingly, we tracked Q_{220} to extract kinetic parameters. Previous studies of cation exchange kinetics with high time resolution by Moser *et al.*[22] used a sum of exponential functions to obtain activation energies based on changes in the bandgap E_g of nanocrystals:

$$E_g = C + \sum_{i=1}^{1,2,3,\ldots} A_i \exp(-k_i t) \qquad (2)$$

Here C is some constant and A_i and k_i are the amplitude and rate constant of the i^{th} process, respectively. **Eqn. 2** is intuitively useful because it describes a sequence of pseudo-first-order reactions, such as the simple metathesis reaction where the concentrations of Cd and Pb in solution are very large and nearly zero, respectively:

$$\mathrm{Cd^{2+}(sol) + PbS \rightarrow CdS + Pb^{2+}(sol)} \qquad (3)$$

However, in fitting Q_{220}, we did not find our data to be well-described by a sum of two exponentials. Specifically, the large scatter of the derived rate constants *k* (especially at high

temperatures) makes any derived activation energies meaningless (**Table S5**, **Fig. S13a**). Furthermore, for the pseudo-first-order approximation (single exponential fit) to apply to our experiments across a given time scale, a large excess of Cd in solution would be required. This condition could not be met here, since a high concentration of PbS NCs was needed for a strong XRD signal (see **Supporting Information**). To account for the changing concentration of Cd, we tried fitting Q_{220} to a second-order rate law (**Table S6**) but also found this to be inadequate, even at low temperatures were stage C would not be operating (**Fig. S13b**).

However, **Fig. 4** and **S3** suggest a rapid approach to a "limiting" value of Q_{220} at very short exchange times, namely during stage **A**. We therefore avoided contributions from successive processes by fitting Q_{220} at very short times (up to about 1000 s, **Fig. 9a**) to a single exponential function. Because stage **A** represents a maximum exchange fraction of about 20%, the concentration of Cd in solution does not change much over this interval. We obtained a reasonably straight Arrhenius plot (**Fig. 9b**, **Table S7-8**) corresponding to an activation energy, E_a, of 41 kJ mol^{-1}. This E_a is similar to those reported for surface exchange or adsorption of ions on NCs (42 [22] to 74 [57] kJ mol^{-1}). Previous calculations of some ionic[58, 59] and molecular[60] binding energies on ionic surfaces have also returned a similar E_a. Some experimental measurements of ion adsorption E_a on solids from solution have found lower values,[61-63] although they are inconsistent in the underlying process to which they attribute E_a (diffusion in solution, physisorption, or chemisorption). Bothe *et al.* examined cation diffusion during exchange in the PbSe-CdSe system and found an E_a of 30-50 kJ mol^{-1}. On the basis of this E_a, they concluded that the transformation proceeded through the diffusion of interstitial cations coupled with a kick-out mechanism, as other processes would require enthalpically unfavorable (E_a > 100 kJ mol^{-1}) vacancy generation within the nanoparticle. However, our results show that exchange up to degrees of 20% conversion for particles of this size can initially occur very rapidly due to replacement of the first few monolayers (0.25 nm) of undercoordinated atoms at the surface, which constitute a significant fraction of the atoms in the NC. Attributing this first step of exchange to a true diffusion process could lead to a misleadingly low activation energy. Additionally, Bothe *et al.* relied on elemental analysis rather than direct structural measures to gauge the progress of exchange, and weakly adsorbed ions or retained Cd precursor could thus contribute to the apparent degree of exchange. On the basis of our E_a, then, we conclude the kinetics of stage **A** describes surface-limited exchange at undercoordinated sites.

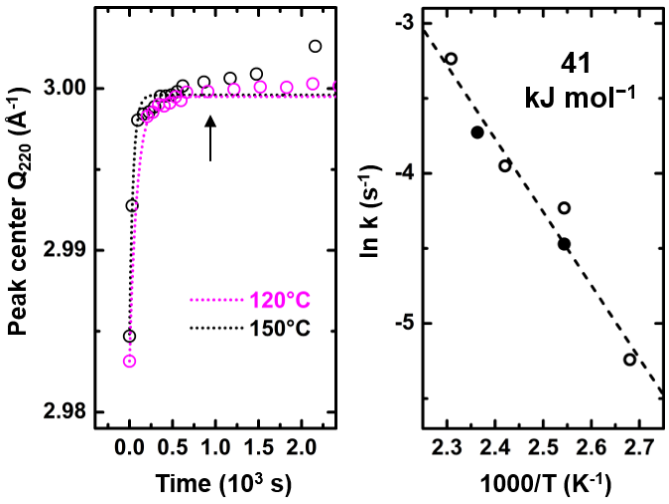

Figure 9. (a) Typical single-exponential fits of the evolution of the (220) peak position for cation exchange at 120 and 150°C (from **Fig. 4**) at very short times (~1000 s, cut-off range indicated by the arrow). An initial rapid shift of Q_{220} occurs (stage **A**) during the initial formation of the rocksalt CdS shell. Q_{220} continues to shift much more slowly (stages B and C) as zincblende CdS is formed. (b) Arrhenius plot of rate constants extracted from (220) data at temperatures 100-160°C. The activation energy is indicated. Data is from two separate experiments: **Fig. 4** (closed points) and **Fig. S3** (open points).

2.10. Quantitation of cation exchange kinetics: stage C

To quantify diffusive transport in our system (stage **C**), we make the key assumption in stage **C** that the shell is conformal to the core and relatively uniform,[15, 16] implying that the relevant transport (diffusion) coefficients, D, for the growth of the shell reflect the diffusivities of the incoming and outgoing components (Cd or Pb, respectively) in the CdS shell. Because the value of D in this experiment should account for the diffusion of both Cd and Pb, we note that our experiment properly measures the interdiffusion coefficient, $\widetilde{D}$. Fick's 2nd law describes the concentration change throughout the nanocrystal

$$\frac{\partial c}{\partial t} = \widetilde{D}\frac{\partial^2 c}{\partial \xi^2}, \tag{4}$$

where c is the concentration of solute, ξ is the spatial coordinate, and t is time. For one-dimensional diffusion, the characteristic time scale for the chemical transformation of a region with length scale ℓ in one dimension follows a parabolic growth law with time:

$$\ell = \sqrt{4\widetilde{D}t}. \tag{5}$$

Fig. 4 shows that the experimental conversion curves do not, in general, have a parabolic dependence on time owing to the spherical geometry and finite size of the NCs and, more significantly, to convolution with processes **A** and **B**. Nevertheless, we can use Fick's law to place our data in the context of previous work on diffusion in nanoparticles. We observe that the driving force for cation exchange under our experimental conditions is large enough that, at high temperatures, exchange does not appear significantly slowed by the depletion of Cd in the

solution until conversion is nearly complete. Because this high driving force must immediately replace outgoing Pb with Cd, we simplify the problem by assuming that Pb from an initially pure PbS particle is lost by diffusion to a solution having an effective Pb concentration of zero. The time scale of the fraction of exchange completed, *X*, can be estimated from the analytical solution (an infinite series in *n*) for diffusion in a spherical particle of radius *R*:[64]

$$X = 1 - \frac{6}{\pi^2}\sum_{n=1}^{\infty}\frac{1}{n^2}\exp\left(-\frac{\widetilde{D}n^2\pi^2 t}{R^2}\right) \quad (6)$$

Here *t* is the experimental time at the point of interest, and *X* can be estimated by interpolating the (220) peak center (Q_{220}) between the bulk values for PbS ($Q^0_{PbS,220}$) and CdS ($Q^0_{CdS,220}$):

$$X = \frac{Q^0_{CdS,220} - Q_{220}}{Q^0_{CdS,220} - Q^0_{PbS,220}} \quad (7)$$

Evaluation of **Eqn. 6** to *n* = 40 was more than sufficient to reach the limits of numerical precision. The resulting interdiffusion coefficients (**Fig. 10** and **Table S9**) range from 10^{-21}-10^{-17} $cm^2\,s^{-1}$ at the lowest and highest temperatures used, respectively. For comparison, on the basis of **Eqn. 5** the interdiffusion coefficient needed for cations to diffuse during exchange to a distance of 3.5 nm in about 5,000 s (e.g., **Fig. 4**, 200°C) is on the order of 10^{-17} cm^2s^{-1}. We also applied a shrinking-core model[65, 66] to determine the diffusion coefficient of Cd through a spherical shell and found values for $\widetilde{D}$ in good agreement with those given by application of Fick's second law (**Fig. 10**, right, **Fig. S14**, and **Table S10**). Therefore, the derived $\widetilde{D}$ is relatively insensitive to the chosen model. More details of the calculations are given in the **Supporting Information**.

2.11. Mechanism of chemical diffusion: magnitude of D̃

Interestingly, our estimated interdiffusion coefficients using Fick's law and the shrinking-core model exceed the range of self-diffusion coefficients for Cd in CdS (wurtzite phase) extrapolated from high-temperature data by four or more orders of magnitude (red area in **Fig. 10a**).[23, 67] Additionally, our interdiffusion coefficients are lower by four orders of magnitude than those for fast-diffusing impurities such as Cu or Li in CdS[67] (gray area in **Fig. 10a**). Reference data are given in **Table S11**. Our measurements indicate that the particles are converted much faster than expected for an ideal solution model using bulk values for the component diffusivity of Cd in CdS would suggest. We were not able to find measurements for the diffusivity of Pb in CdS; however, due to the larger size of the Pb^{2+} cation relative to Cd^{2+}, we expected that its diffusivity in CdS (rocksalt or zincblende) would be reduced. DFT calculations to check the activation barriers to diffusion, ΔH_{diff}, for neutral vacancies and interstitials (**Table S4**) returned values in agreement with our expectations. Values of ΔH_{diff} in PbS and in both rs-CdS and zb-CdS are very similar for Cd and Pb (vacancy-mediated diffusion) or substantially larger for Pb relative to Cd (interstitial-mediated). Our measurements of the diffusion coefficient do fall within a range of values reported for self-diffusion of Pb in PbS[68] (blue area in **Fig. 10a**). This surprising observation suggests, counter-intuitively, that diffusion through the PbS template might be a rate-limiting process. Experimental evidence presented previously does not appear to rule this out. In Pb chalcogenides, cation exchange is associated with an increase in core polydispersity and displacement of the core from the center of the particle, sometimes to the extent that the "core" continues to form part of the surface.[19, 20] However, since the PbS@CdS

system has not been observed (by us or by others) to form Janus-type structures following addition of Cd^{2+} to PbS,[17, 19] bulk-like diffusion in PbS appears unlikely to be the main rate-controlling process. If the CdS shell is conformal and uniform, then our results find accelerated diffusion by up to four orders of magnitude in $\widetilde{D}$ in the CdS shell at short length scales (up to 3.5 nm) relative to expectations from bulk measurements.

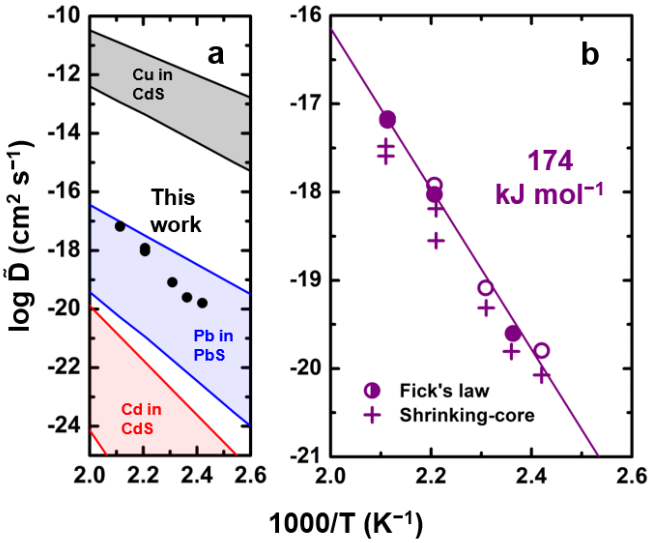

Figure 10. Arrhenius plots of interdiffusion coefficients, $\tilde{D}$, for ionic transport (Pb and Cd diffusion through shell) extracted from (220) data at temperatures above 140°C and at long exchange times. In (a) points are given on an expanded scale to place the data in context with other measurements of self-diffusion coefficients (see main text). In (b) the points are given on a compact scale; the activation energy is indicated. Points in (b) indicate $\tilde{D}$ as determined using Fick's second law (circles) and the shrinking-core model (crosses). Closed points: from data of **Fig. 4**; open points: from data of **Fig. S3**. Reference data is extrapolated from high temperature data described in **Table S11**.

The nature of the interdiffusion coefficient $\widetilde{D}$ should be clarified. The self-diffusion coefficients in **Fig. 10** were obtained under conditions close to thermodynamic equilibrium where no chemical potential gradient exists (i.e. in a tracer experiment). Cation exchange in nanocrystals clearly does not reflect such a situation. The fluxes of Pb and Cd atoms in this case are coupled such that Cd displaces Pb in a one-to-one ratio, in spite of the fact that their component diffusion coefficients, D_{Cd} and D_{Pb}, are not, in general, expected to be equal. For an ideal solution of the two components in each other where the internal electric fields in the NC do not play a role, $\widetilde{D}$ would change with the phase fraction of Cd X_{Cd} in the following way:[69]

$$\widetilde{D} = D_{Pb}X_{Cd} + D_{Cd}X_{Pb} \quad (8)$$

Here $X_{Pb} = 1-X_{Cd}$. Excess defect generation in the NC might also need to be considered to understand $\widetilde{D}$. A notable example of the consequences of unequal component diffusivities is the nanoscale Kirkendall effect, where unequal diffusivities of anions and cations require the generation of vacancies in the cores of NCs to balance the outgoing cation flux.[70, 71] Cation exchange in the PbS-to-CdS system does not exhibit such behavior, but other routes exist for

coupling of cation fluxes. For example, if Cd diffuses more rapidly than Pb, interdiffusion at a PbS-CdS interface will lead to Cd penetrating further into PbS than Pb in CdS, leading to a net separation of charge at the interface. This gives rise to an electric field that opposes the further separation of charge. To preserve local electroneutrality, $\widetilde{D}$ takes a different form:[69]

$$\widetilde{D} = \frac{D_{Pb}D_{Cd}}{D_{Pb}X_{Pb} + D_{Cd}X_{Cd}} \tag{9}$$

Given the small size of the system and the small value of the bandgap E_g for PbS, we expect that the number of thermally generated charge carriers would be sufficient to satisfy the electroneutrality condition for any diffusion into PbS. The situation for zb-CdS, which has a larger bandgap, is not clear. For both **Eqn. 8** and **Eqn. 9**, suppose D_{Pb} and D_{Cd} in a hypothetical $Pb_{1-x}Cd_xS$ ideal solution take their values for the self-diffusion coefficients given in **Fig. 10a**, which is reasonable in the limit of dilute impurities in a solid. Then for X_{Cd} = 1 (the assumed case for a zb-CdS shell containing a negligible amount of Pb) $\widetilde{D}$ has the value of D_{Pb}, which is, coincidentally, in agreement with our experimental magnitude of $\widetilde{D}$. Thus, the transport of the minority (slowest) component controls the overall rate of the exchange.

2.12. Chemical diffusion in nanocrystals: possible enhancement factors

However, the different structures for pure PbS and CdS in our NCs and the immiscibility of CdS and PbS in the bulk[34] indicate that the PbS-CdS system does not follow ideal solution behavior. Moreover, in nanoscale systems, impurities generally are not isolated (or dilute). The ideal solution interdiffusion coefficient, $\widetilde{D}_0$ must be modified by a thermodynamic factor[69, 72] (*e.g.* for Cd):

$$\widetilde{D} = \widetilde{D}_0\left(1 + \frac{\mathrm{d}\ln\gamma_{Cd}}{\mathrm{d}\ln X_{Cd}}\right) \tag{10}$$

γ_{Cd} is the activity ($a_{Cd} = \gamma_{Cd}X_{Cd}$) coefficient of Cd. A crucial problem in describing diffusion in semiconductors is that component activity depends very strongly on the external conditions owing to deviations in stoichiometry and changes in dopant concentrations (in bulk solids). As a result, the thermodynamic factor can be very large with minuscule changes in composition and, in fact, can greatly exceed our reported factor of 10^4 difference between $\widetilde{D}$ and the self-diffusion coefficients D_{Cd}.[73] It therefore seems that the large chemical driving force, with the resulting bias in diffusive jumps, could account for the apparently enhanced diffusivity in cation exchange without invoking nanoscale effects such as quantum confinement. However, the distinction between chemical diffusion and self-diffusion is often not made in the nanoparticle literature. A careful description of defect and component activities in nanostructures will be crucial to elucidating true transport coefficients in future work.

We mention some other factors that could contribute to enhanced diffusion in NCs. Chan *et al.* argued that coupling of point defects to surface vibrations in NCs (breathing modes) could greatly reduce diffusion barriers in small (less than 2 nm in diameter) CdSe NCs.[12] Our PbS@CdS core-shell particles, however, are much larger, and the effect of such vibrations on diffusion barriers well below the surface of the NC is likely to be minimal. The contribution of strain at the PbS-CdS interface to observed mixing could also be significant, since strain accommodation has been observed in many systems to take place through a degree of interface alloying. Such diffuse interfaces have been shown in some systems to extend over a

few nm or more.[74] Diffusion through extended defects, such as grain boundaries, is a third possibility. Such high-diffusivity paths[72] are especially important in diffusion at low temperatures. The role of such paths in cation exchange has, in general, not been appreciated, which might be surprising given the loss in crystalline perfection that is observed in many cases of cation exchange, including the PbS-CdS system. If Pb leaves *via* the surface faster than arriving Cd can diffuse through the shell, transport through high-diffusivity paths, such as dislocations in the growing shell or along the PbS-CdS interface, could still provide Cd more quickly than can bulk-like ionic transport. Accordingly, the increased magnitude of the diffusion coefficient relative to bulk self-diffusion of Cd in CdS could reflect the introduction of a high concentration of extended defects, in accordance with the substantial (2.2%) lattice mismatch between PbS and zincblende CdS. We were unable to distinguish clearly any grain boundaries or stacking faults in our NCs (**Fig. 7**), but Bals et al. have identified stacking faults unambiguously in PbSe@CdSe nanocrystals, along with phase boundaries with displaced anionic sublattices.[44] To separate the chemical diffusion factor from contributions of high-conductivity paths, better high-resolution structural studies (*i.e.* through TEM) on more particles are necessary to quantify the extent of such paths as grain boundaries or stacking faults in the shell. This will be particularly important in investigating the feasibility of a "layer-by-layer" exchange mechanism proposed to explain pronounced anisotropy of exchange even in cubic materials.[19, 44]

Future experiments are necessary to examine the contribution of the large chemical potential gradient in cation exchange relative to the expected defect structure in the shell. We suggest that at length scales where the chemical potential gradient can be made small due to the low solubility of the two exchanging phases (the dilute solution limit) and where lattice strain can be completely accommodated (perhaps longer than 5 nm), the kinetics of diffusion should slow greatly. Further work in, for example, x-ray reflectivity measurements on PbS-CdS surfaces or diffusion experiments on larger particles would furnish quantitative results on the necessary length scale. Observation by these means of a drastic drop in the apparent rate of diffusion for thick layers would lend credence to previous suggestions that cation exchange in PbS@CdS[15, 19, 56] or in very large nanoparticles[3] is "self-limiting." Similarly, in systems where no lattice strain or boundaries between immiscible phases is present to induce defect formation, transformation should reflect the kinetics of diffusion in the bulk solid. Diffusion experiments on slightly larger length scales could also offer insight into how the point defect structure of nanoparticles depends on their size.

2.13. Mechanism of diffusion: Arrhenius parameters

In spite of the expected contributions to the kinetics of diffusion from the factors above, we can still examine the activation barriers, E_a, to the diffusion reaction to gain some insight into the reaction mechanism. An Arrhenius plot of the effective interdiffusion coefficients determined at temperatures greater than 140°C is given in **Fig. 10b**. Where identical temperatures were investigated in the two different experiments we carried out, the points are in excellent agreement with each other. Two different models (Fick's second law and the shrinking-core model) return nearly identical values for E_a (**Table S12**), with a fit of all measured interdiffusion coefficients in **Fig. 10b** giving an E_a of 174 (Fick's law) or 165 kJ mol^{-1} (shrinking-core). At high temperatures, the E_a of 174 kJ mol^{-1} exceeds reported values of E_a for the diffusion of Cd in CdS determined from the sulfidation of large Cd nanoparticles (106 kJ mol^{-1}),[75] from the diffusion of Mn^{2+} in CdSe (also 106 kJ mol^{-1}),[21] and the diffusion of Cd or Pb in CdSe (40-50 kJ mol^{-1}).[1] A more similar value of 154 kJ mol^{-1} has been reported for the interdiffusion of CdSe-

ZnSe.[76] Our activation energy is closer to some measured values of 179-258 kJ mol^{-1} for the diffusion of Cd in wurtzite CdS[23, 67] or of 98-146 kJ mol^{-1} for Pb in PbS.[68] Theoretical predictions give a very wide range of values for point defect formation energies, so that it may not be possible to make an assignment with certainty. Our measured E_a is also less than some predictions for the enthalpies of formation for point defects such as Schottky pairs,[77] which are generally >400 kJ mol^{-1} (for a two-atom defect). It is important to note that previous experimental observations on diffusion in nanoparticles generally measured E_a as a combination of the energies for defect formation, ΔH_f, and migration, ΔH_m. More reliable data exist for Cd in wurtzite CdS[23] and indicate that ΔH_f tends to be large (>100 kJ mol^{-1}) regardless of the type of defect (interstitial or vacancy), while ΔH_m can be of the same order of magnitude but in the case of interstitial diffusion is often much smaller.[67] Since our E_a remains large, we conclude that the ΔH_f of a defect such as a Cd vacancy or Pb interstitial is a major contributor to the diffusion activation energy in our case. Theoretical simulations of diffusion migration barriers in nanoparticles[9, 71] also support this conjecture. Although our DFT simulations seem to explain the presence of a rocksalt layer in the PbS-CdS heterosystem, we are less successful in determining activation energy barriers for diffusion. The estimated $\Delta H = \Delta H_f + \Delta H_m$ for diffusion was universally >200 kJ mol^{-1} (**Table S3-4**) and exceeded considerably the measured values of E_a in our system for all paths considered (Cd or Pb interstitials or vacancies in PbS, zincblende CdS, or rocksalt CdS). We do note, however, that the lowest observed barrier is for Cd interstitial diffusion in rocksalt CdS at 209 kJ mol^{-1}. It is interesting to consider this in light of the possibility that a high-diffusivity path may be involved in atomic transport. The interfacial rocksalt CdS layer posited to exist following further growth of the shell might serve this role.

Finally, we consider the pre-exponential factor, $\tilde{D}_0$, in the Arrhenius expression for the interdiffusion coefficient (**Table S12**). The corresponding $\tilde{D}_0$ for **Fig. 10b** is $1.1 \cdot 10^2$ (Fick's law) or 3.3 cm^{2}s^{-1} (shrinking-core). This value is rather large compared to numerous other measurements for ionic self-diffusion in semiconductor systems[23, 68] and for chemical diffusion in nanoparticles,[21, 75] which generally find values for a prefactor ranging from 10^{-7} to 10^{-3} cm^{2}s^{-1}. However, some measurements of self-diffusion in bulk solids give similar or even slightly larger values of D_0 (up to about 10^3 cm^{2}s^{-1}).[67] D_0 provides key information in this case, because the attempt frequency giving rise to D_0 in solids is related to a characteristic vibration frequency (Γ) on the order of $10^{11\text{-}13}$ s^{-1}.[72] In pure stoichiometric substances, the diffusion coefficient is proportional to Γ times the square of the jump length a_0:

$$D_0 \propto a_0^2 \Gamma \tag{11}$$

In solid-state diffusion mediated by point defect transport, a_0 is necessarily on the order of the unit cell length (a few Å), and the theoretical prefactor is therefore about 10^{-4} to 10^{-2} cm^{2}s^{-1}, or several orders of magnitude below our measured $\tilde{D}_0$. An enhanced value of $\tilde{D}_0$ could arise from an increase in the jump length due to the presence of extended defects, as we mentioned above. However, the magnitude of such an enhancement is ostensibly limited by the size of the system. As the size of the nanocrystals here is only a factor of 10 larger than a jump length between lattice sites, the increase in the a_0^2 term in **Eqn. 11** is only 10^2, which may be too small to explain the increase in $\tilde{D}_0$ observed here. An increase in the effective Γ, or a "biased" jump frequency, may originate from the thermodynamic factor mentioned above (**Eqn. 10**). Specifically, the concentration of defects may greatly exceed that expected from the enthalpy of defect formation, $\exp(-\Delta H_f/kT)$, owing to the presence of impurities or other changes in the external chemical boundary conditions that act to stabilize defects by charge compensation or

other mechanisms.[72] This further supports our conclusion that the small size of the region for diffusion leads to the significant enhancement of diffusive transport in NCs over length scales of a few nanometers due to the very large chemical potential gradients developed across the surface-shell-core region.

3. Conclusion

X-ray diffraction characterization of lead sulfide (PbS) nanocrystals (NCs) undergoing transformation to cadmium sulfide (CdS) reveals that the cation exchange reaction proceeds in three stages with a complex series of intermediates. Upon the initial introduction of Cd (stage **A**), a thin shell of CdS rapidly develops on the surface of PbS. We confirm unambiguously that this shell adopts a metastable rocksalt phase (rs-CdS) from peak position and intensity shifts in agreement with those given by Debye scattering equation simulations, from Raman spectroscopy, and from density functional theory (DFT) simulations. This phase may persist as an interlayer throughout the exchange, raising the possibility that such interfaces can be made to serve useful roles in tuning the complex electronic structure of nanocrystalline heterostructures. As the shell grows and the overlying CdS recrystallizes (stage **B**) to the stable zincblende phase (zb-CdS), the peak intensities and positions become more like those of simulated PbS@zb-CdS particles, and we observe unusual diffraction effects manifesting as anomalous peak shifts. We identify such behaviors as emerging naturally from the commensurate relationship between rocksalt PbS and zincblende CdS cation sublattices and show that such a relationship serves to break the symmetry of the core-shell quantum dot without requiring an actual change in unit cell space group. During the third stage, **C**, the remainder of the particle is converted to zb-CdS *via* diffusive transport through the outer layers of the particle. The kinetics of the cation exchange reaction can be quantified using parameters from the XRD data that are insensitive to the particular phase of CdS. The kinetics of the cation exchange are complex and a number of processes contribute, so that the overall activation energies of the exchange at high and low temperatures appear to be different. However, using very general diffusion models, we estimate that interdiffusion coefficients in the PbS-CdS system, even at diffusion lengths larger than a few monolayers, are increased by a few orders of magnitude relative to those estimated from high-temperature data for self-diffusion of Cd in CdS. The interdiffusion coefficients have a large Arrhenius activation energy in comparison to several other reports of diffusion in nanoparticles, and we suggest that convolution of diffusion with surface reactions could produce anomalously low activation energies. However, the magnitude of the interdiffusion coefficient is still much larger than values for self-diffusion in CdS, and the major cause of accelerated diffusion appears to be the very large chemical potential gradient involved in cation exchange, which by definition requires a change in the activities of component ions from zero to unity over a very short distance. Such an enhancement can be expressed as a contributing thermodynamic factor in the interdiffusion coefficient, which can, for example, reflect a change in stoichiometry. Diffusion through high-conductivity paths is also a possible explanation, due to the significant lattice mismatch between PbS and CdS, and increases the distance that atoms with every diffusive jump. It is important to recognize the profound difference between experimental configurations with and without a chemical potential gradient and to provide much more detailed characterization of such factors as component activity and defect structure for quantifying transport coefficients of matter at the nanoscale.

Acknowledgements

This work was supported in part by the National Science Foundation (NSF) under award numbers CHE-1507753, CHE-1665305, and DMR-1542776. This work made use of the Cornell Center for Materials Research shared facilities, which are supported through the NSF MRSEC program (DMR-1719875), and the Cornell High Energy Synchrotron Source (CHESS) facilities, which are supported by the NSF (DMR-1332208). This work also made use of the computational resources provided by the University of Florida Research Computing Center. We thank S. Stoupin, D. Smilgies, and A. Itskovich (CHESS) for assistance with x-ray experiments, J. Kopsa and J. Houghton (CHESS) for preparation of apparatus, and R. Dieckmann (Cornell Materials Science and Engineering) for helpful discussions. We also thank S. Giri (Cornell Biological and Environmental Engineering) for an elemental analysis.

Supporting Information

Available online in the Electronic Supporting Information (ESI): Experimental procedures, background on kinetic parameter determination, computational details, Figures **S1** through **S14**, and **Tables S1** through **S12**. This material is available free of charge *via* the Internet at http://pubs.acs.org.

References

1. Bothe, C.; Kornowski, A.; Tornatzky, H.; Schmidtke, C.; Lange, H.; Maultzsch, J.; Weller, H., Solid-State Chemistry on the Nanoscale: Ion Transport through Interstitial Sites or Vacancies? *Angewandte Chemie International Edition* **2015,** 54, 14183-14186.
2. Beberwyck, B. J.; Surendranath, Y.; Alivisatos, A. P., Cation Exchange: A Versatile Tool for Nanomaterials Synthesis. *Journal of Physical Chemistry C* **2013,** 117, 19759-19770.
3. Son, D. H.; Hughes, S. M.; Yin, Y.; Paul Alivisatos, A., Cation exchange reactions in ionic nanocrystals. *Science* **2004,** 306, 1009-1012.
4. Robinson, R. D.; Sadtler, B.; Demchenko, D. O.; Erdonmez, C. K.; Wang, L.-W.; Alivisatos, A. P., Spontaneous superlattice formation in nanorods through partial cation exchange. *Science* **2007,** 317, 355-358.
5. Li, H.; Zanella, M.; Genovese, A.; Povia, M.; Falqui, A.; Giannini, C.; Manna, L., Sequential cation exchange in nanocrystals: preservation of crystal phase and formation of metastable phases. *Nano Letters* **2011,** 11, 4964-4970.
6. Fenton, J. L.; Steimle, B. C.; Schaak, R. E., Tunable intraparticle frameworks for creating complex heterostructured nanoparticle libraries. *Science* **2018,** 360, 513-517.
7. Pietryga, J. M.; Werder, D. J.; Williams, D. J.; Casson, J. L.; Schaller, R. D.; Klimov, V. I.; Hollingsworth, J. A., Utilizing the lability of lead selenide to produce heterostructured nanocrystals with bright, stable infrared emission. *Journal of the American Chemical Society* **2008,** 130, 4879-4885.
8. Kroupa, D. M.; Hughes, B. K.; Miller, E. M.; Moore, D. T.; Anderson, N. C.; Chernomordik, B. D.; Nozik, A. J.; Beard, M. C., Synthesis and Spectroscopy of Silver-Doped PbSe Quantum Dots. *Journal of the American Chemical Society* **2017,** 139, 10382-10394.
9. Ha, D.-H.; Caldwell, A. H.; Ward, M. J.; Honrao, S.; Mathew, K.; Hovden, R.; Koker, M. K. A.; Muller, D. A.; Hennig, R. G.; Robinson, R. D., Solid−Solid Phase Transformations Induced through Cation Exchange and Strain, in 2D Heterostructured Copper Sulfide Nanocrystals. *Nano Letters* **2014,** 14, 7090-7099.
10. Maier, J., Point-defect thermodynamics and size effects. *Solid State Ionics* **2000,** 131, 13-22.

11. Dalpian, G. M.; Chelikowsky, J. R., Self-purification in semiconductor nanocrystals. *Physical Review Letters* **2006,** 96, 226802.
12. Chan, T. L.; Zayak, A. T.; Dalpian, G. M.; Chelikowsky, J. R., Role of confinement on diffusion barriers in semiconductor nanocrystals. *Physical Review Letters* **2009,** 102, 025901.
13. Neo, D. C. J.; Cheng, C.; Stranks, S. D.; Fairclough, S. M.; Kim, J. S.; Kirkland, A. I.; Smith, J. M.; Snaith, H. J.; Assender, H. E.; Watt, A. A. R., Influence of Shell Thickness and Surface Passivation on PbS/CdS Core/Shell Colloidal Quantum Dot Solar Cells. *Chemistry of Materials* **2014,** 26, 4004-4013.
14. Zhao, H.; Chaker, M.; Ma, D., Effect of CdS shell thickness on the optical properties of water-soluble, amphiphilic polymer-encapsulated PbS/CdS core/shell quantum dots. *Journal of Materials Chemistry* **2011,** 21, 17483-17491.
15. Justo, Y.; Sagar, L. K.; Flamee, S.; Zhao, Q.; Vantomme, A.; Hens, Z., Less is more. Cation exchange and the chemistry of the nanocrystal surface. *ACS Nano* **2014,** 8, 7948-7957.
16. Justo, Y.; Geiregat, P.; Hoecke, K. V.; Vanhaecke, F.; De Mello Donega, C.; Hens, Z., Optical Properties of PbS/CdS Core/Shell Quantum Dots. *Journal of Physical Chemistry C* **2013,** 117, 20171-20177.
17. Lechner, R. T.; Fritz-Popovski, G.; Yarema, M.; Heiss, W.; Hoell, A.; Schülli, T. U.; Primetzhofer, D.; Eibelhuber, M.; Paris, O., Crystal Phase Transitions in the Shell of PbS/CdS Core/Shell Nanocrystals Influences Photoluminescence Intensity. *Chemistry of Materials* **2014,** 26, 5914-5922.
18. Hewavitharana, I. K.; Brock, S. L., When Ligand Exchange Leads to Ion Exchange: Nanocrystal Facets Dictate the Outcome. *ACS Nano* **2017,** 11, 11217–11224.
19. Casavola, M.; van Huis, M. A.; Bals, S.; Lambert, K.; Hens, Z.; Vanmaekelbergh, D., Anisotropic Cation Exchange in PbSe/CdSe Core/Shell Nanocrystals of Different Geometry. *Chemistry of Materials* **2012,** 24, 294-302.
20. Lambert, K.; De Geyter, B.; Moreels, I.; Hens, Z., PbTe|CdTe Core|Shell Particles by Cation Exchange, a HR-TEM study. *Chemistry of Materials* **2009,** 21, 778-780.
21. Chakraborty, P.; Jin, Y.; Barrows, C. J.; Dunham, S. T.; Gamelin, D. R., Kinetics of Isovalent (Cd^{2+}) and Aliovalent (In^{3+}) Cation Exchange in $Cd_{1-x}Mn_xSe$ Nanocrystals. *Journal of the American Chemical Society* **2016,** 138, 12885-12893.
22. Moser, A.; Yarema, M.; Lin, W. M. M.; Yarema, O.; Yazdani, N.; Wood, V., In Situ Monitoring of Cation-Exchange Reaction Shell Growth on Nanocrystals. *The Journal of Physical Chemistry C* **2017,** 121, 24345-24351.
23. Kumar, V.; Kröger, F. A., Self-diffusion and the defect structure of cadmium sulfide. *Journal of Solid State Chemistry* **1971,** 3, 387-400.
24. Van Dyck, D.; Van Tendeloo, G.; Amelinckx, A., Diffraction effects due to a single translation interface in a small crystal. *Ultramicroscopy* **1984,** 15, 357-370.
25. Qadri, S. B.; Yang, J. P.; Skelton, E. F.; Ratna, B. R., Evidence of strain and lattice distortion in lead sulfide nanocrystallites. *Applied Physics Letters* **1997,** 70, 1020-1021.
26. Bertolotti, F.; Dirin, D. N.; Ibáñez, M.; Krumeich, F.; Cervellino, A.; Frison, R.; Voznyy, O.; Sargent, E. H.; Kovalenko, M. V.; Guagliardi, A.; Masciocchi, N., Crystal symmetry breaking and vacancies in colloidal lead chalcogenide quantum dots. *Nature Materials* **2016,** 15, 987-994.
27. Hendricks, M. P.; Campos, M. P.; Cleveland, G. T.; Jen-La Plante, I.; Owen, J. S., A tunable library of substituted thiourea precursors to metal sulfide nanocrystals. *Science* **2015,** 348, 1226-1230.
28. Huang, F.; Banfield, J., Size-Dependent Phase Transformation Kinetics in Nanocrystalline ZnS. *Journal of the American Chemical Society* **2005,** 127, 4523-4529.
29. Spurr, R. A.; Myers, H., Quantitative Analysis of Anatase-Rutile Mixtures with an X-ray Diffractometer. *Analytical Chemistry* **1957,** 29, 760-762.

30. Abel, K. A.; FitzGerald, P. A.; Wang, T.-Y.; Regier, T. Z.; Raudsepp, M.; Ringer, S. P.; Warr, G. G.; van Veggel, F. C. J. M., Probing the Structure of Colloidal Core/Shell Quantum Dots Formed by Cation Exchange. *Journal of Physical Chemistry C* **2012,** 116, 3968–3978.
31. Gilbert, B.; Zhang, H.; Chen, B.; Kunz, M.; Huang, F.; Banfield, J. F., Compressibility of zinc sulfide nanoparticles. *Physical Review B* **2006,** 74, 115405.
32. Hamachi, L. S.; Plante, I. J.-L.; Coryell, A. C.; Roo, J. D.; Owen, J. S., Kinetic Control over CdS Nanocrystal Nucleation Using a Library of Thiocarbonates, Thiocarbamates, and Thioureas. *Chemistry of Materials* **2017,** 29, 8711–8719.
33. Peters, J. L.; van den Bos, K. H. W.; Van Aert, S.; Goris, B.; Bals, S.; Vanmaekelbergh, D., Ligand-Induced Shape Transformation of PbSe Nanocrystals. *Chemistry of Materials* **2017,** 29, 4122-4128.
34. Bethke, P. M.; Barton, P. B., Sub-solidus relations in the system PbS-CdS. *American Mineralogist* **1971,** 1971, 2034-2039.
35. Shibata, T.; Bunker, B. A.; Zhang, Z.; Meisel, D.; Vardeman, C. F.; Gezelter, J. D., Size-Dependent Spontaneous Alloying of Au−Ag Nanoparticles. *Journal of the American Chemical Society* **2002,** 124, 11989–11996.
36. Jesser, W. A.; Schamp, C. T., Nanoparticle semiconductor compositions in the miscibility gap. *physica status solidi c* **2008,** 5, 539-544.
37. Burch, D.; Bazant, M. Z., Size-Dependent Spinodal and Miscibility Gaps for Intercalation in Nanoparticles. *Nano Letters* **2009,** 9, 3795–3800.
38. Groiss, H.; Hesser, G.; Heiss, W.; Schäffler, F.; Leitsmann, R.; Bechstedt, F.; Koike, K.; Yano, M., Coherent {001} interfaces between rocksalt and zinc-blende crystal structures. *Physical Review B* **2009,** 79, 235331.
39. Chuang, C.-H. M.; Brown, P. R.; Bulović, V.; Bawendi, M. G., Improved performance and stability in quantum dot solar cells through band alignment engineering. *Nature Materials* **2014,** 13, 796-801.
40. Lai, L.-H.; Protesescu, L.; Kovalenko, M. V.; Loi, M. A., Sensitized solar cells with colloidal PbS–CdS core–shell quantum dots. *Physical Chemistry Chemical Physics* **2014,** 16, 736-742.
41. Tolbert, S. H.; Herhold, A. B.; Johnson, C. S.; Alivisatos, A. P., Comparison of Quantum Confinement Effects on the Electronic Absorption Spectra of Direct and Indirect Gap Semiconductor Nanocrystals. *Physical Review B* **1994,** 73, 3266-3269.
42. Martín-Rodríguez, R.; González, J.; Valiente, R.; Aguado, F.; Santamaría-Pérez, D.; Rodríguez, F., Reversibility of the zinc-blende to rock-salt phase transition in cadmium sulfide nanocrystals. *Journal of Applied Physics* **2012,** 111, 063516.
43. Alayoglu, S.; Zavalij, P.; Eichhorn, B.; Wang, Q.; Frenkel, A.; Chupas, P., Structural and Architectural Evaluation of Bimetallic Nanoparticles: A Case Study of Pt−Ru Core−Shell and Alloy Nanoparticles. *ACS Nano* **2009,** 3, 3127-3137.
44. Bals, S.; Casavola, M.; Huis, M. A. v.; Aert, S. V.; Batenburg, K. J.; Tendeloo, G. V.; Vanmaekelbergh, D., Three-Dimensional Atomic Imaging of Colloidal Core-Shell Nanocrystals. *Nano letters* **2011,** 11, 3420-3424.
45. Guinier, A., *X-Ray diffraction in crystals, imperfect crystals, and amorphous bodies*. Dover: Mineola, New York, 1994.
46. Ovsyannikov, S. V.; Ponosov, Y. S.; Shchennikov, V. V.; Mogilenskikh, V. E., Raman spectra of lead chalcogenide single crystals. *physica status solidi c* **2004,** 1, 3110-3113.
47. Krauss, T. D.; Wise, F. W.; Tanner, D. B., Observation of Coupled Vibrational Modes of a Semiconductor Nanocrystal. *Physical Review Letters* **1996,** 76, 1376-1379.
48. Blackburn, J. L.; Chappell, H.; Luther, J. M.; Nozik, A. J.; Johnson, J. C., Correlation between Photooxidation and the Appearance of Raman Scattering Bands in Lead Chalcogenide Quantum Dots. *Journal of Physical Chemistry Letters* **2011,** 2, 599-603.

49. Batonneau, Y.; Bremard, C.; Laureyns, J.; Merlin, J. C., Microscopic and imaging Raman scattering study of PbS and its photo-oxidation products. *Journal of Raman Spectroscopy* **2000,** 31, 1113-1119.
50. Dzhagan, V. M.; Valakh, M. Y.; Milekhin, A. G.; Yeryukov, N. A.; Zahn, D. R. T.; Cassette, E.; Pons, T.; Dubertret, B., Raman- and IR-Active Phonons in CdSe/CdS Core/Shell Nanocrystals in the Presence of Interface Alloying and Strain. *Journal of Physical Chemistry C* **2013,** 117, 18225–18233.
51. Chen, Y.; Vela, J.; Htoon, H.; Casson, J. L.; Werder, D. J.; Bussian, D. A.; Klimov, V. I.; Hollingsworth, J. A., "Giant" Multishell CdSe Nanocrystal Quantum Dots with Suppressed Blinking. *Journal of the American Chemical Society* **2008,** 130, 5026–5027.
52. Nan, W.; Niu, Y.; Qin, H.; Cui, F.; Yang, Y.; Lai, R.; Lin, W.; Peng, X., Crystal Structure Control of Zinc-Blende CdSe/CdS Core/Shell Nanocrystals: Synthesis and Structure-Dependent Optical Properties. *Journal of the American Chemical Society* **2012,** 134, 19685−19693.
53. Gong, K.; Kelley, D. F., Lattice Strain Limit for Uniform Shell Deposition in Zincblende CdSe/CdS Quantum Dots. *Journal of Physical Chemistry Letters* **2015,** 6, 1559-1562.
54. Cretí, A.; Zavelani-Rossi, M.; Lanzani, G.; Anni, M.; Manna, L.; Lomascolo, M., Role of the shell thickness in stimulated emission and photoinduced absorption in CdSe core/shell nanorods. *Physical Review B* **2006,** 73, 165410.
55. Koscher, B. A.; Bronstein, N. D.; Olshansky, J. H.; Bekenstein, Y.; Alivisatos, A. P., Surface- vs Diffusion-Limited Mechanisms of Anion Exchange in $CsPbBr_3$ Nanocrystal Cubes Revealed through Kinetic Studies. *Journal of the American Chemical Society* **2016,** 138, 12065-12068.
56. Fan, Z.; Lin, L.-C.; Buijs, W.; Vlugt, T. J. H.; van Huis, M. A., Atomistic understanding of cation exchange in PbS nanocrystals using simulations with pseudoligands. *Nature Communications* **2016,** 7, 11503.
57. Roy, S.; Bhandari, S.; Chattopadhyay, A., Quantum Dot Surface Mediated Unprecedented Reaction of Zn^{2+} and Copper Quinolate Complex. *Journal of Physical Chemistry C* **2015,** 119, 21191–21197.
58. Erwin, S. C.; Zu, L.; Haftel, M. I.; Efros, A. L.; Kennedy, T. a.; Norris, D. J., Doping semiconductor nanocrystals. *Nature* **2005,** 436, 91-94.
59. Kerisit, S.; Parker, S. C., Free Energy of Adsorption of Water and Metal Ions on the {10-14} Calcite Surface. *Journal of the American Chemical Society* **2004,** 126, 10152-10161.
60. Murphy, R.; Strongin, D. R., Surface reactivity of pyrite and related sulfides. *Surface Science Reports* **2009,** 64, 1-45.
61. Boparai, H. K.; Joseph, M.; O'Carroll, D. M., Kinetics and thermodynamics of cadmium ion removal by adsorption onto nano zerovalent iron particles. *Journal of Hazardous Materials* **2011,** 186, 458-465.
62. Lakshmipathiraj, P.; Narasimhan, B. R. V.; Prabhakar, S.; Raju, G. B., Adsorption of arsenate on synthetic goethite from aqueous solutions. *Journal of Hazardous Materials* **2006,** 136, 281-287.
63. Argun, M. E., Use of clinoptilolite for the removal of nickel ions from water: Kinetics and thermodynamics. *Journal of Hazardous Materials* **2008,** 150, 587-595.
64. Crank, J., *The mathematics of diffusion*. 2nd ed.; Clarendon Press: Oxford, 1975.
65. Ethayaraja, M.; Bandyopadhyaya, R., Model for Core−Shell Nanoparticle Formation by Ion-Exchange Mechanism. *Industrial & Engineering Chemistry Research* **2008,** 47, 5982-5985.
66. Levenspiel, O., *Chemical Reaction Engineering*. 3rd ed.; John Wiley and Sons: New York, 1999.
67. Fedorov, V. A.; Ganshin, V. A.; Korkishko, Y. N., Ion Exchange in II-VI Crystals: Thermodynamics, Kinetics, and Technology. *physica status solidi a* **1993,** 139, 9-65.

68. Simkovich, G.; Wagner, J. B., Self-Diffusion of Lead 210 in Single Crystals of Lead Sulfide as a Function of Stoichiometry and Doping Additions. *Journal of Chemical Physics* **1963,** 38, 1368-1375.
69. Mehrer, H., *Diffusion in Solids*. Springer: Heidelberg, 2007.
70. Yin, Y.; Rioux, R. M.; Erdonmez, C. K.; Hughes, S.; Somorjai, G. A.; Alivisatos, A. P., Formation of hollow nanocrystals through the nanoscale Kirkendall effect. *Science* **2004,** 304, 711-714.
71. Ha, D.-H.; Moreau, L. M.; Honrao, S.; Hennig, R. G.; Robinson, R. D., The Oxidation of Cobalt Nanoparticles into Kirkendall-Hollowed CoO and Co_3O_4: The Diffusion Mechanisms and Atomic Structural Transformations. *Journal of Physical Chemistry C* **2013,** 117, 14303-14312.
72. Shewmon, P. G., *Diffusion in Solids*. 2nd ed.; Minerals, Metals, & Materials Society: Warrendale, Pa., 1989.
73. Stevenson, D. A., Diffusion in the Chalcogenides of Zn, Cd, and Pb. In *Atomic Diffusion in Semiconductors*, Shaw, D., Ed. Plenum Publishing Company: New York, 1973.
74. Nakagawa, N.; Hwang, H. Y.; Muller, D. A., Why some interfaces cannot be sharp. *Nature Materials* **2006,** 5, 204-209.
75. Cabot, A.; Smith, R. K.; Yin, Y.; Zheng, H.; Reinhard, B. M.; Liu, H.; Alivisatos, A. P., Sulfidation of Cadmium at the Nanoscale. *ACS Nano* **2008,** 2, 1452-1458.
76. Sung, Y.-M.; Lee, Y.-J.; Park, K.-S., Kinetic Analysis for Formation of $Cd_{1-x}Zn_xSe$ Solid-Solution Nanocrystals. *Journal of the American Chemical Society* **2006,** 128, 9002-9003.
77. Wright, K.; Gale, J. D., Interatomic potentials for the simulation of the zinc-blende and wurtzite forms of ZnS and CdS: Bulk structure, properties, and phase stability. *Physical Review B* **2004,** 70, 035211.

TOC figure